Published in final edited form as:

Oncogene. 2017 July 06; 36(27): 3807–3819. doi:10.1038/onc.2017.23.

EGFR-mediated Macrophage Activation Promotes Colitis-associated Tumorigenesis

Dana M. Hardbower[1,2], **Lori A. Coburn**[2,4,6], **Mohammad Asim**[2], **Kshipra Singh**[2], **Johanna C. Sierra**[2], **Daniel P. Barry**[2], **Alain P. Gobert**[2,4], **M. Blanca Piazuelo**[2,4], **M. Kay Washington**[1], and **Keith T. Wilson**[1,2,3,4,5,6,*]

[1]Department of Pathology, Microbiology and Immunology; Vanderbilt University Medical Center; Nashville, TN, USA

[2]Division of Gastroenterology, Hepatology and Nutrition, Department of Medicine; Vanderbilt University Medical Center; Nashville, TN, USA

[3]Department of Cancer Biology; Vanderbilt University Medical Center; Nashville, TN, USA

[4]Center for Mucosal Inflammation and Cancer, Vanderbilt University Medical Center; Nashville, TN, USA

[5]Vanderbilt Ingram Cancer Center; Vanderbilt University Medical Center; Nashville, TN, USA

[6]Veterans Affairs Tennessee Valley Healthcare System; Nashville, TN, USA

Abstract

Epidermal growth factor receptor (EGFR) signaling is a known mediator of colorectal carcinogenesis. Studies have focused on the role of EGFR signaling in epithelial cells, although the exact nature of the role of EGFR in colorectal carcinogenesis remains a topic of debate. Here, we present evidence that EGFR signaling in myeloid cells, specifically macrophages, is critical for colon tumorigenesis in the AOM-DSS model of colitis-associated carcinogenesis (CAC). In a human tissue microarray, colonic macrophages demonstrated robust EGFR activation in the pre-cancerous stages of colitis and dysplasia. Utilizing the AOM-DSS model, mice with a myeloid-specific deletion of *Egfr* had significantly decreased tumor multiplicity and burden, protection from high-grade dysplasia, and significantly reduced colitis. Intriguingly, mice with gastrointestinal epithelial cell-specific *Egfr* deletion demonstrated no differences in tumorigenesis in the AOM-DSS model. The alterations in tumorigenesis in myeloid-specific *Egfr* knockout mice were accompanied by decreased macrophage, neutrophil, and T cell infiltration. Pro-tumorigenic M2 macrophage activation was diminished in myeloid-specific *Egfr*-deficient mice, as marked by decreased *Arg1* and *Il10* mRNA expression and decreased IL-4, IL-10 and IL-13 protein levels.

*CORRESPONDING AUTHOR Keith T. Wilson, MD, 2215 Garland Avenue, 1030C Medical Research Building IV, Nashville, TN 37232, Phone: 615-343-5675, keith.wilson@vanderbilt.edu.

CONFLICT OF INTEREST

The authors declare that no conflict of interest exists.

SUPPLEMENTARY INFORMATION

Supplementary Information accompanies the paper on the *Oncogene* website (http://nature.com/onc).

Surprisingly, diminished M1 macrophage activation was also detectable, as marked by significantly reduced *Nos2* and *Il1b* mRNA levels and decreased IFN-γ, TNF-α, and IL-1β protein levels. The alterations in M1 and M2 macrophage activation were confirmed in bone marrow-derived macrophages from mice with the myeloid-specific *Egfr* knockout. The combined effect of restrained M1 and M2 macrophage activation resulted in decreased production of pro-angiogenic factors, CXCL1 and VEGF, and reduced $CD31^+$ blood vessels, which likely contributed to protection from tumorigenesis. These data reveal that EGFR signaling in macrophages, but not in colonic epithelial cells, has a significant role in CAC. EGFR signaling in macrophages may prove to be an effective biomarker of CAC or target for chemoprevention in patients with inflammatory bowel disease.

Keywords

Macrophage activation; colon cancer; EGFR; angiogenesis; inflammation; tumorigenesis

INTRODUCTION

Colorectal cancer is the third most common cancer globally[1] and accounts for approximately 10% of new cancer diagnoses annually[1]. The risk for colon carcinogenesis is linked to chronic inflammatory states, such as inflammatory bowel disease (IBD)[2-4]. Colitis-associated carcinogenesis (CAC) occurs in 20% of patients diagnosed with IBD, and mortality rates are over 50% in these patients[2-4]. While mechanisms by which chronic inflammation promotes colonic carcinogenesis are being investigated[2-4], unanswered questions remain.

The tumor microenvironment contains various immune cell types, including macrophages[2-4]. Macrophages represent a heterogeneous subset of innate immune cells with roles in tissue homeostasis, pro-inflammatory and anti-microbial responses, and wound repair[5-7], and are of particular interest given their highly plastic phenotypes that can both promote and inhibit tumorigenesis[8,9]. Macrophages can alter their function based on the activation program utilized – either M1 or M2 patterns[5-7,10]. M1 macrophages are pro-inflammatory, anti-microbial, and thought to be anti-tumorigenic, although this remains the subject of debate[5-7]. M2 macrophages are associated with wound healing and have pro-tumorigenic properties[5,8,10]. Macrophage activation is dependent upon the colon tumor microenvironment[9,11,12] and pathways that regulate this are incompletely understood[3,8]. Studies have implicated nuclear factor kappa-light-chain-enhancer of activated B cells (NF-κB) signaling[13-15] and other pathways[16,17].

We recently demonstrated that epidermal growth factor receptor (EGFR) signaling regulates macrophage activation across various stimuli[18]. EGFR phosphorylation occurs in macrophages and has major effects on expression of both M1 and M2 macrophage activation markers[18]. Importantly, we determined that EGFR signaling occurs in human gastric macrophages from gastritis to gastric adenocarcinoma[18], leading us to speculate that EGFR signaling in macrophages may also have a role in CAC. EGFR signaling has been most commonly studied within the context of epithelial cell function and has been linked to

colorectal cancer initiation and progression[19-21]. The impact of EGFR protein levels and signaling capacity is an area of ongoing investigation[19-21].

Here, we demonstrate that EGFR signaling in macrophages has a profound effect on development of CAC. Early, inflammation-mediated stages of colon carcinogenesis in humans were marked by EGFR phosphorylation in macrophages. Myeloid-specific *Egfr* knockout mice exhibited decreased tumor multiplicity and tumor burden, while epithelial-specific *Egfr* knockout mice had no differences in phenotype. Loss of *Egfr* in myeloid cells resulted in decreased M2 and M1 macrophage activation, and decreased angiogenesis. Thus, EGFR signaling in macrophages may represent a potential target for therapeutic intervention in CAC.

RESULTS

EGFR signaling occurs in human colonic macrophages during pre-cancerous stages of CAC

The majority of studies related to EGFR signaling during CRC have focused on epithelial cells[19-23]. Instead, we sought to determine if human colonic macrophages had detectable levels of phospho-EGFR (pEGFR), a marker of active EGFR signaling, during IBD and associated CAC. We utilized an IBD-associated cancer tissue microarray (TMA) from Vanderbilt University Medical Center, which contained cases of inactive and active ulcerative colitis, dysplasia, and colitis-associated carcinoma[25]. pEGFR levels in $CD68^+$ macrophages were detected via immunofluorescence staining (Figure 1a) and quantified with CellProfiler image analysis software (http://www.cellprofiler.com). We observed a low percentage of $CD68^+pEGFR^+$ macrophages in inactive colitis that was significantly increased in active colitis and dysplasia (Figure 1b, c). The percentage of $CD68^+pEGFR^+$ macrophages was lower in CAC than in active colitis and dysplasia (Figure 1b, c). The histopathologic diagnosis of inactive colitis indicates an absence of neutrophils, but is typically characterized by expansion of the lamina propria immune cell compartment and relative dropout of the epithelium. As such, no differences in the overall percentage of macrophages were detected between disease groups (Supplementary Figure 1). These data indicate that pEGFR is present in macrophages during pre-cancerous events associated with colonic inflammation, implying that EGFR signaling in macrophages has an important role in macrophage function during initiation of carcinogenesis. It should be noted that, as expected, pEGFR staining was also abundant in colonic epithelial cells (CECs; Figure 1a).

EGFR signaling in macrophages contributes to AOM-DSS-induced colon tumorigenesis

We next sought to directly determine the role of EGFR signaling in macrophages during colon carcinogenesis. We utilized mice containing myeloid-specific, *Egfr* deletion ($Egfr^{\Delta mye}$) driven by LysM-Cre, which we have extensively characterized in models of gastric and colonic inflammation[18], and the appropriate control mice ($Egfr^{fl/fl}$). $Egfr^{fl/fl}$ and $Egfr^{\Delta mye}$ mice were subjected to the azoxymethane (AOM)-dextran sodium sulfate (DSS) model of CAC[27,28]. The AOM-DSS protocol utilized is outlined in Supplementary Figure 2. No tumors were observed in the AOM-only or DSS-only groups, nor were differences in histologic colitis detectable between genotypes in the DSS-only group (data not shown). The

lack of difference in the histologic colitis between genotypes in the DSS-only group is likely due to the prolonged recovery period, resulting in low colitis scores. Only data from the control and AOM-DSS groups are presented herein.

AOM-DSS-treated *Egfr*$^{\Delta mye}$ mice had significantly decreased tumor multiplicity and tumor burden, measured as the sum of the area of each tumor, versus AOM-DSS-treated *Egfr*$^{fl/fl}$ mice (Figure 2a, b). Further, *Egfr*$^{\Delta mye}$ mice were significantly protected from development of high-grade dysplasia, developing a maximum of low-grade dysplasia (Figure 2c). Representative hematoxylin and eosin (H&E)-stained images demonstrate the decrease in tumor size and protection from high-grade dysplasia in *Egfr*$^{\Delta mye}$ mice (Figure 2d). The myeloid-specific, *Egfr* knockout was maintained throughout the entire AOM-DSS protocol, as immunofluorescence images reveal the presence of many CD68^{+}total EGFR (tEGFR)$^{+}$ colonic macrophages in tissues from AOM-DSS-treated *Egfr*$^{fl/fl}$ mice, while only CD68^{+}tEGFR^{-} colonic macrophages are detectable in *Egfr*$^{\Delta mye}$ tissues (Figure 2e). Taken together, these data indicate that EGFR in myeloid cells is a potent promoter of tumorigenesis in mice.

Additionally, *Egfr*$^{\Delta mye}$ mice demonstrated significantly decreased histologic colitis with AOM-DSS versus *Egfr*$^{fl/fl}$ mice (Figure 2f). In conjunction with decreased histologic colitis, *Egfr*$^{\Delta mye}$ mice exhibited significant protection from weight loss associated with each cycle of DSS, as compared to *Egfr*$^{fl/fl}$ mice (Figure 2g). These data indicate that *Egfr*$^{\Delta mye}$ mice are protected from the pro-inflammatory effects of the AOM-DSS model, which contributes to decreased CAC.

To assess the role of epithelial-specific EGFR in colon tumorigenesis, *Foxa3*$^{cre/+}$ mice were crossed with *Egfr*$^{fl/fl}$ mice. *Foxa3* is expressed in all gastrointestinal epithelial cells from mouth to anus[24,29]. Isolated, naïve CECs from *Egfr*$^{fl/fl}$ mice crossed with *Foxa3*$^{cre/+}$ mice demonstrated absence of tEGFR (Supplementary Figure 3a). Despite a report indicating that *Foxa3* is expressed in hematopoietic progenitor cells[30], we found no detectable deletion of EGFR in naïve splenocytes (Supplementary Figure 3b), or bone marrow-derived macrophages (BMmacs; Supplementary Figure 3c). Thus, we termed these mice *Egfr*$^{\Delta GIepi}$, indicative of the epithelial-specific *Egfr* deletion in the gastrointestinal tract. It should be noted that direct comparisons of *Egfr*$^{\Delta mye}$ mice and *Egfr*$^{\Delta GIepi}$ mice are not possible because *Egfr*$^{\Delta GIepi}$ mice are on a mixed background, while *Egfr*$^{\Delta mye}$ mice are on a congenic C57BL/6 background.

When subjected to the AOM-DSS protocol, *Egfr*$^{fl/fl}$ (littermate controls of the *Egfr*$^{\Delta GIepi}$ mice, and not the same as *Egfr*$^{fl/fl}$ mice utilized in studies with *Egfr*$^{\Delta mye}$ mice) and *Egfr*$^{\Delta GIepi}$ mice exhibited no differences in tumor multiplicity and tumor burden (Supplementary Figure 4a, b). Moreover, *Egfr*$^{fl/fl}$ and *Egfr*$^{\Delta GIepi}$ mice had similar susceptibility to low- and high-grade dysplasia (Supplementary Figure 4c). Representative H&E-stained images reveal tumors of similar size and severity of dysplasia (Supplementary Figure 4d).

Lack of differences between *Egfr*$^{fl/fl}$ and *Egfr*$^{\Delta GIepi}$ mice could be due to inefficient CRE-mediated excision of *Egfr*. However, loss of EGFR signaling was maintained in *Egfr*$^{\Delta GIepi}$

epithelial cells during AOM-DSS treatment (Supplementary Figure 4e). pEGFR immunoperoxidase staining is robust in epithelial cells and immune cells in *Egfr*$^{fl/fl}$ mice, but is restricted to immune cells in *Egfr*$^{\Delta GIepi}$ mice (Supplementary Figure 4e). In addition, no differences were observed in histologic colitis between *Egfr*$^{fl/fl}$ and *Egfr*$^{\Delta GIepi}$ mice (Supplementary Figure 4f). *Egfr*$^{fl/fl}$ and *Egfr*$^{\Delta GIepi}$ mice also displayed similar weight loss during each cycle of DSS (Supplementary Figure 4g). Taken together, EGFR signaling in immune cells, but not in epithelial cells, is critical for the promotion of tumorigenesis in mice.

EGFR signaling in macrophages enhances the innate immune response in colon tumors

The AOM-DSS model utilizes inflammation to drive tumorigenesis[27,28,31]. Based on decreased histologic colitis, combined with decreased tumor multiplicity and burden in *Egfr*$^{\Delta mye}$ mice, we sought to determine the nature of the innate immune response within the tumor microenvironment during AOM-DSS-induced CAC. We assessed 32 cytokines/chemokines via Luminex Multiplex Array. Analytes that were not different between genotypes or undetectable are in Supplementary Table 1.

The C-C ligand (CCL) chemokines CCL3 (MIP-1α) and CCL4 (MIP-1β) protein levels were significantly decreased in *Egfr*$^{\Delta mye}$ tumors versus *Egfr*$^{fl/fl}$ tumors (Figure 3a). CCL3 and CCL4 are chemoattractants for innate immune cells, and are produced by macrophages[32]. Additionally, levels of the C-X-C ligand (CXCL) chemokines, CXCL9 (MIG) and CXCL10 (IP-10), were diminished in *Egfr*$^{\Delta mye}$ tumors (Figure 3a). CXCL9 and CXCL10 are also primarily produced by macrophages[33], but induce T cells infiltration[34]. CCL3, CCL4, CXCL9, and CXCL10 were induced to a similar degree in *Egfr*$^{fl/fl}$ and *Egfr*$^{\Delta GIepi}$ tumors, and no differences were detected between genotypes (Supplementary Figure 5a). Taken together, the decreases in CCL3, CCL4, CXCL9, and CXCL10 are indicative of decreased macrophage responses that result in decreased innate and adaptive immune cell infiltration in tumor areas. These significant decreases in macrophage-driven immune responses indicate the essential role of myeloid EGFR in driving CAC.

In addition, *Egfr*$^{\Delta mye}$ tumors demonstrated significant differences in cytokine levels (Figure 3b, c). Leukemia inhibitory factor (LIF), a cytokine with pleiotropic effects on immune function, was decreased in *Egfr*$^{\Delta mye}$ tumors (Figure 3b). LIF protein levels were induced to a similar degree in *Egfr*$^{fl/fl}$ and *Egfr*$^{\Delta GIepi}$ tumors (Supplementary Figure 5b). LIF overexpression is associated with poor prognosis in colorectal cancer[35,36], and decreased LIF levels in *Egfr*$^{\Delta mye}$ tumors are consistent with the decreased tumor multiplicity and burden. Moreover, colony stimulating factor 1 (CSF1; M-CSF) and interleukin (IL)-1α were significantly decreased in *Egfr*$^{\Delta mye}$ tumors (Figure 3c), but not altered between *Egfr*$^{fl/fl}$ and *Egfr*$^{\Delta GIepi}$ tumors (Supplementary Figure 5c). CSF1 and IL-1α are produced by activated macrophages[15,37-39], and CSF1 represents a key factor in macrophage activation and downstream function. Taken together, the decreases in these three cytokines indicate an overall downregulation of immune/inflammatory responses within tumors lacking EGFR in myeloid cells, and imply that macrophage EGFR is a central driver of tumorigenesis in an inflammation-dependent model.

To further investigate the effects of reduced chemokine production, we assessed populations of immune cells by immunohistochemistry with the following markers: macrophages (CD68), neutrophils (myeloperoxidase, MPO), T cells (CD3), and B cells (CD45R). Abundance of these cells was scored in non-tumor and tumor tissue, and combined for an overall score. Consistent with decreased CCL3 and CCL4 levels (Figure 3a), there were significantly diminished macrophages and neutrophils in AOM-DSS-treated *Egfr*$^{\Delta mye}$ mice versus *Egfr*$^{fl/fl}$ mice (Figure 4a, b). T cell abundance was also significantly decreased in AOM-DSS-treated *Egfr*$^{\Delta mye}$ mice (Figure 4c), consistent with diminished CXCL9 and CXCL10 in these mice (Figure 3a). B cells were not different between genotypes (Figure 4d). Taken together, these data show diminished immune cell infiltration in the *Egfr*$^{\Delta mye}$ mice, which is dependent upon EGFR signaling in myeloid cells.

EGFR signaling in macrophages enhances M2 activation in colon tumors

Because macrophages were likely the major source of several of the chemokines and cytokines which were significantly reduced in *Egfr*$^{\Delta mye}$ tumors, we hypothesized that loss of EGFR led to altered macrophage activation in the tumor microenvironment. M2 macrophages are tumor-associated macrophages and have pro-tumorigenic properties[5-7,10]. Thus, the decrease in tumor multiplicity and burden could be due to a diminished M2 macrophage response in *Egfr*$^{\Delta mye}$ tumors.

Indeed, protein levels of IL-4, IL-10, and IL-13, drivers of M2 activation[5-7,10], were significantly upregulated in *Egfr*$^{fl/fl}$ tumors and decreased in *Egfr*$^{\Delta mye}$ tumors (Figure 5a). Moreover, mRNA levels of the M2 markers, arginase 1 (*Arg1*) and *Il10*, were also increased in *Egfr*$^{fl/fl}$ tumors and decreased in *Egfr*$^{\Delta mye}$ tumors (Figure 5b). Significant decreases in both the levels of cytokines that induce M2 activation and the expression of M2 macrophage markers indicate diminished M2 macrophage activation in *Egfr*$^{\Delta mye}$ mice, consistent with reduced colon tumorigenesis.

Egfr$^{fl/fl}$ and *Egfr*$^{\Delta GIepi}$ tumors did not demonstrate differences in IL-4 or IL-10 levels (Supplementary Figure 6a), nor were differences detectable in *Arg1* and *Il10* mRNA levels (Supplementary Figure 6b). IL-13 was detected at very low levels in *Egfr*$^{fl/fl}$ and *Egfr*$^{\Delta GIepi}$ tumors, but no significant differences were detected (Supplementary Table 2). These data correlate with the finding that *Egfr*$^{fl/fl}$ and *Egfr*$^{\Delta GIepi}$ mice do not have significant differences in development of CAC.

To confirm that *Egfr* deletion in myeloid cells resulted in decreased M2 activation, we isolated BMmacs from *Egfr*$^{fl/fl}$ and *Egfr*$^{\Delta mye}$ mice and stimulated them *ex vivo* with IL-4 and IL-10. Markers of M2 macrophage activation were assessed by qRT-PCR. IL-4/IL-10 stimulation led to a significant induction of *Arg1*, chitinase-like 3 (*Chil3*), and *Il10* in both *Egfr*$^{fl/fl}$ and *Egfr*$^{\Delta mye}$ BMmacs (Figure 5c). Importantly, *Arg1*, *Chil3*, and *Il10* mRNA levels were significantly decreased in *Egfr*$^{\Delta mye}$ BMmacs (Figure 5c), consistent with the findings in *Egfr*$^{\Delta mye}$ tumors. Together, these data further suggest that EGFR signaling regulates M2 macrophage activation.

To address the mechanism by which macrophage EGFR signaling alters M2 activation, we isolated BMmacs from *Egfr*$^{fl/fl}$ and *Egfr*$^{\Delta mye}$ mice, stimulated them *ex vivo* with IL-4, and

assessed phospho-signal transducer and activator of transcription 6 (STAT6), a known mediator of M2 activation[40]. *Egfr*$^{\Delta mye}$ BMmacs exhibited decreased pSTAT6 levels when compared to *Egfr*$^{fl/fl}$ BMmacs (Figure 5d). Similarly, AOM-DSS-treated *Egfr*$^{\Delta mye}$ tissues demonstrated reduced pSTAT6 levels in immune cells (Figure 5e). These data reveal a potential link between EGFR and STAT6 in regulating M2 activation in macrophages.

Macrophage-specific EGFR signaling also augments M1 activation in colon tumors

Alterations in M2 macrophage activation in *Egfr*$^{\Delta mye}$ mice were not unexpected, given the close association between M2 macrophages and the tumor microenvironment[8,9]. However, we also observed significant alterations in both the levels of cytokines that induce M1 activation and in M1 markers in *Egfr*$^{\Delta mye}$ tumors.

Interferon (IFN)-γ and tumor necrosis factor (TNF)-α potently induce M1 macrophage activation[7]. Protein levels of both IFN-γ and TNF-α were significantly upregulated in AOM-DSS-induced tumors in *Egfr*$^{fl/fl}$ mice and significantly reduced in *Egfr*$^{\Delta mye}$ tumors (Figure 6a), indicative of decreased capacity for M1 macrophage activation. mRNA levels of M1 markers nitric oxide synthase 2 (*Nos2*) and *Il1b* were upregulated in *Egfr*$^{fl/fl}$ tumors, and significantly decreased in *Egfr*$^{\Delta mye}$ tumors (Figure 6b). This decrease in M1 macrophage activation was confirmed at the protein level, as IL-1β protein was also significantly decreased in *Egfr*$^{\Delta mye}$ tumors (Figure 6c). Protein levels of IFN-γ and TNF-α were detectable in *Egfr*$^{fl/fl}$ and *Egfr*$^{\Delta GIepi}$ tumors, but were not different between genotypes (Supplementary Figure 7a). mRNA levels of *Nos2* and *Il1b* (Supplementary Figure 7b), as well as IL-1β protein levels, were upregulated in *Egfr*$^{fl/fl}$ and *Egfr*$^{\Delta GIepi}$ tumors, but again were not different between genotypes.

To assess the role of EGFR signaling in M1 activation, we isolated BMmacs from *Egfr*$^{fl/fl}$ and *Egfr*$^{\Delta mye}$ mice and stimulated *ex vivo* with IFN-γ and TNF-α for 24 h. M1 stimulation resulted in robust expression of M1 markers *Nos2*, *Il1b*, and *Tnfa* (Figure 6d). Importantly, mRNA expression of *Nos2*, *Il1b*, and *Tnfa* was significantly reduced in *Egfr*$^{\Delta mye}$ BMmacs versus *Egfr*$^{fl/fl}$ BMmacs (Figure 6d), indicating that EGFR signaling is equally critical for M1 and M2 activation. Intriguingly, M1 activation may have critical role in colon tumorigenesis in this model that is regulated by EGFR signaling.

We have previously demonstrated that EGFR signaling is upstream of NF-κB in macrophages during *Helicobacter pylori* infection[18]. Moreover, we have reported that there is enhanced nuclear translocation of RELA proto-oncogene, NF-κB subunit (RELA; also known as p65) in two different models of colitis[41]. Thus, we hypothesized that EGFR and NF-κB signaling may regulate M1 activation. We isolated BMmacs from *Egfr*$^{fl/fl}$ and *Egfr*$^{\Delta mye}$ mice, stimulated with IFN-γ and lipopolysaccharide, and assessed phospho-RELA (pRELA) levels. *Egfr*$^{\Delta mye}$ BMmacs had diminished pRELA levels versus *Egfr*$^{fl/fl}$ BMmacs (Figure 6e). Moreover, AOM-DSS-treated *Egfr*$^{\Delta mye}$ tissues had markedly decreased RELA nuclear translocation in lamina propria cells (Figure 6f). Thus, EGFR signaling activates the NF-κB pathway to regulate M1 activation.

EGFR signaling in macrophages enhances angiogenesis in colon tumors

Angiogenesis is a hallmark of carcinogenesis[42], and is an essential means by which colon tumor growth is supported[43,44]. Several cytokines, including vascular endothelial growth factor (VEGF) A and CXCL1 (KC, GRO-α), the murine equivalent of CXCL8 (IL-8)[45], contribute to angiogenesis[46-49]. M1 macrophages are an important source of CXCL1[26] and both M1 and M2 macrophages are important sources of VEGFA[50].

Based on i) decreased tumor multiplicity/burden, and ii) decreased M2 and M1 macrophage activation in *Egfr*$^{\Delta mye}$ mice, we hypothesized that angiogenesis may be impaired, contributing to diminished tumorigenesis. *Egfr*$^{\Delta mye}$ tumors had decreased mRNA levels of *Cxcl1* and *Vegfa* (Figure 7a) and altered protein levels of CXCL1 and VEGF (Figure 7b) versus *Egfr*$^{fl/fl}$ tumors. *Egfr*$^{fl/fl}$ and *Egfr*$^{\Delta GIepi}$ tumors did not demonstrate any differences in mRNA or protein levels of these markers (Supplementary Figure 8). Additionally, M1-activated *Egfr*$^{\Delta mye}$ BMmacs expressed significantly less *Cxcl1* and *Vegfa* (Supplementary Figure 9a) and M2-activated *Egfr*$^{\Delta mye}$ BMmacs expressed less *Vegfa* (Supplementary Figure 9b) versus *Egfr*$^{fl/fl}$ BMmacs. These data confirm that macrophages are a potential source of CXCL1 and VEGF, and that EGFR signaling is critical for expression of these pro-angiogenic mediators.

To confirm that decreased pro-angiogenic cytokines was accompanied by decreased angiogenesis, we performed immunoperoxidase staining for CD31, a marker of vascular endothelial cells[51]. Representative images demonstrate significantly enhanced angiogenesis in AOM-DSS-treated *Egfr*$^{fl/fl}$ versus *Egfr*$^{\Delta mye}$ mice (Figure 7c). Notably, angiogenesis in AOM-DSS-treated *Egfr*$^{\Delta mye}$ mice was not different than angiogenesis in control *Egfr*$^{fl/fl}$ and *Egfr*$^{\Delta mye}$ mice (Figure 7c). Both the number of CD31^{+} blood vessels per case (Figure 7d) and the total area of CD31^{+} blood vessels (Figure 7e) were significantly decreased in AOM-DSS-treated *Egfr*$^{\Delta mye}$ mice versus *Egfr*$^{fl/fl}$ mice. Thus, decreases in pro-angiogenic cytokine production were associated with decreased angiogenesis in *Egfr*$^{\Delta mye}$ mice. Decreased angiogenesis likely contributed to diminished tumorigenesis in this CAC model.

DISCUSSION

EGFR signaling is a commonly studied pathway in carcinogenesis[19,20,52-54], although most studies related to EGFR signaling have been performed in epithelial cells[19,20,52-54]. This study outlines an important role for EGFR signaling in macrophages during inflammatory colon tumorigenesis. Herein, we demonstrate that EGFR signaling occurs in human macrophages during pre-cancerous stages of ulcerative colitis and dysplasia, both of which are marked by active inflammation[3,4]. Based on diminished CD68^{+}pEGFR^{+} cells in CAC, we posit that EGFR signaling in human macrophages may be essential for initiation of inflammation-associated tumorigenesis. Myeloid-specific knockout of *Egfr* significantly protected mice from tumorigenesis in the AOM-DSS model of CAC. Intriguingly, gastrointestinal epithelial cell-specific knockout of *Egfr* did not have a phenotype that was significantly different from wild-type mice. Protection from tumorigenesis in *Egfr*$^{\Delta mye}$ mice was accompanied by restricted M2 and M1 macrophage activation, which likely contributed to decreased angiogenesis due to less production of pro-angiogenic cytokines and

chemokines. These data point to a currently underappreciated role for EGFR signaling in myeloid cells, particularly macrophages, in promoting CAC.

A previous study utilizing *Wa5* mice, which carry a dominant-negative allele that impairs EGFR signaling, demonstrated that EGFR signaling inhibited CAC[55], the opposite of our current result. It should be noted that differences in colon tumorigenesis were only significant when *Wa5* mice were crossed with *Il10*$^{-/-}$ mice[55]. *Il10*$^{-/-}$ mice may have limitations as a model for CAC, because effects of the *Il10* deletion can be modulated by bacterial infections[56,57]. The AOM-DSS model is solely dependent upon inflammation as a driver of carcinogenesis[56,57]. The previous work that demonstrated a protective role for EGFR in colon tumorigenesis also utilized the AOM-DSS model of colon tumorigenesis, but noted no significant differences in tumor multiplicity[55]. Moreover, the *Wa5* allele affects all cell types, while our models used herein were myeloid- and gastrointestinal epithelial-cell-specific. Taken together, our study provides a strong body of evidence that EGFR signaling in macrophages is a critical component of CAC.

EGFR signaling appears to mediate M1 and M2 macrophage activation. Importantly, we demonstrated via multiple methods in a previously published study that EGFR signaling in macrophages had no effect on apoptosis[18]. Thus, the phenotypes observed are due to alterations in macrophage function, not cell viability. While the finding that decreased M2 activation, which is highly pro-tumorigenic[8,10,52], correlated with decreased tumor multiplicity and burden was not unexpected, the dramatic alteration of M1 activation was somewhat surprising. However, there are potential reasons why M1 activation may have an important role in tumorigenesis. Firstly, as we demonstrated, M1 macrophages are an important source of pro-angiogenic cytokines (VEGF) and chemokines (CXCL1). Secondly, M1 macrophages are a potent source of NOS2 (as shown herein) and nitric oxide (NO)[6,7,18]. It has been proposed that NO, a reactive nitrogen species, promotes colon tumorigenesis by causing DNA mutations and DNA instability[3,58]. Our work demonstrates that EGFR signaling has a role in promoting both M1 and M2 activation, potentially working synergistically to promote colon tumorigenesis.

In sum, our study outlines a novel role for EGFR signaling in macrophages during CAC. Robust EGFR signaling in human macrophages in stages leading to colitis-associated cancer indicates that macrophage pEGFR may serve as a potential biomarker for CRC risk in colitis patients. Moreover, our previous work showed that TNF-α induced EGFR signaling in macrophages[18]. Thus, one potential benefit of anti-TNF treatment, frequently used in IBD patients, may be suppression of macrophage EGFR signaling. Further studies are imperative to further assess the critical role that EGFR activation plays in immune cells in patients at risk for progression to colon cancer.

MATERIALS AND METHODS

Reagents

Reagents used for cell culture were from Invitrogen (Carlsbad, CA, USA). Reagents for RNA extraction were from Qiagen (Valencia, CA, USA); those for cDNA synthesis and qRT-PCR were from Bio-Rad (Hercules, CA, USA). Murine M-CSF, IFN-γ, IL-4, and IL-10

were from PeproTech (Rocky Hill, NJ, USA). Murine TNF-α was from Thermo Fisher Scientific (Waltham, MA, USA). Azoxymethane and LPS were from Sigma-Aldrich (St. Louis, MO, USA). DSS was from TdB Consultancy (Uppsala, Sweden).

Antibodies

See **Supplementary Table 4** for information regarding antibodies.

Cells and Culture Conditions

BMmacs were isolated and differentiated from murine femurs as described[18,59]. Red blood cells were lysed in ammonium-chloride-potassium buffer for 3 min, and 1.25 million cells were differentiated with 20 μg/mL recombinant murine M-CSF for 7 days, with media changes at days 3 and 5. Following differentiation, cells were placed in complete Dulbecco's modified Eagle's medium (DMEM), supplemented with 10% fetal bovine serum, 2 mM L-glutamine, 25 mM HEPES, and 10 mM sodium pyruvate for studies with IFN-γ, TNF-α, IL-4, IL-10, or LPS. Stimulation times and doses are indicated in figure legends.

Animal Studies

Egfr$^{fl/fl}$ and *Egfr*$^{\Delta mye}$ mice were utilized as described[18]. C57BL/6 *Egfr*$^{fl/fl}$ mice were crossed with C57BL/6 *LysM*$^{cre/cre}$ mice to generate myeloid-specific, *Egfr* deletion (*Egfr*$^{\Delta mye}$). C57BL/6 *Egfr*$^{fl/fl}$ mice were crossed to CD-1/DBA *Foxa3*$^{cre/+}$ mice obtained from Timothy Wang (Columbia University Medical Center)[60], to generate *Egrf*$^{\Delta GIepi}$ mice. As *Egrf*$^{\Delta GIepi}$ mice contain one *Cre* allele, littermates were utilized for all experiments. Animals were used under protocol M/10/155, approved by the Institutional Animal Care and Use Committee at Vanderbilt University.

Male mice, aged 6-12 weeks, were utilized for all studies. Samples sizes were based on previous AOM-DSS studies from our laboratory. Mice were not removed from the cages into which they were weaned. No other criteria were utilized for selection or randomization. Mice were subjected to the azoxymethane (AOM)-dextran sodium sulfate (DSS) colon tumorigenesis model[27,61]. Mice received one intraperitoneal AOM injection (12.5 mg/kg) on Day 0, and three doses of 4% DSS in their drinking water on Days 5, 26, and 47. The first two cycles of DSS lasted for 5 days, and the third for 4 days. Mice were weighed every 7 days from the start of the first DSS cycle and on Day 0 to determine the AOM dosage. Mice were sacrificed on Day 77.

Rarely, *Egfr*$^{\Delta mye}$ mice developed an enlarged spleen that was not attributable to AOM-DSS treatment. These mice were excluded from further analysis.

Tumor multiplicity was determined by visual inspection via dissecting microscope. Tumor burden was determined by the summation of tumor area, assessed by electronic caliper. Histologic colitis and dysplasia were determined by a gastrointestinal pathologist, M.K.W., in a blinded manner.

Human Tissues

The IBD-associated CAC human TMA was utilized as described[25].

Real-Time PCR

RNA was isolated from cells and tissues as described[18,59]. cDNA was prepared and PCR was performed as described[18,59]. See **Supplementary Table 3** for primers utilized.

Western Blot Analysis

Western blot analysis was performed as described[18,59].

Luminex Multiplex Array

Luminex Multiplex Array was performed as described[18,59]. Tissues were harvested at time of sacrifice, homogenized via a handheld homogenizer in 300 μL CellLytic MT Cell Lysis Reagent (Sigma) and centrifuged at 14,000*g* at 4°C twice. All kit instructions were followed in the performance of the Luminex Multiplex Array assay.

Immunofluorescence Staining for tEGFR and CD68, and RELA

Staining for tEGFR and CD68 in both the TMA and in murine tissues was performed as described[18], with the following exceptions in murine tissue. An initial blocking step was performed with Background Sniper (Biocare Medical), followed by incubation with anti-tEGFR. A second blocking step was performed with the Fab fragment of murine IgG for 15 min, followed 3% goat serum for 15 min, with subsequent incubation with anti-CD68. All other steps were as described. RELA staining and confocal microscopy was performed as described[41].

Immunoperoxidase Staining for pEGFR Y1068

Staining for pEGFR in human colonic biopsies was performed as described[52].

Immunoperoxidase Staining

CD68, MPO, and pSTAT6—After overnight heating at 37°C, sections were deparaffinized in xylene and rehydrated in graded alcohols. Sections were incubated with primary antibody overnight at room temperature. After washing, incubation with anti-rabbit HRP-polymer was performed for 30 min. Sections were rinsed and incubated with streptavidin-HRP (Biocare Medical, Concord, CA, USA) for 30 min.

CD3, CD45R, and CD31—Heat-induced antigen retrieval was performed on the Leica Bond Max using Epitope Retrieval 2 solution for 10 min (CD3, CD31) and 20 min (CD45R). Slides were incubated with primary antibody for 1 h and incubated with secondary antibody for 15 min. CD31 Images were captured using a high throughput Leica SCN400 Slide Scanner automated digital image system. Tissue samples were mapped using Ariol® Review software. The numbers and areas of $CD31^+$ blood vessels were determined in the Ariol® software.

Scoring of CD68, MPO, CD3, and CD45R Immunoperoxidase Staining

Slides were scored in a blinded manner by a gastrointestinal pathologist (M.B.P.). Samples were evaluated for staining in non-tumor and tumor areas using the following scale: 0=scarce positive cells, 1=low abundance of positive cells, 2=moderate abundance of

positive cells, and 3=high abundance of positive cells. The two scores were combined for a highest possible score of 6.

Purification of colonic epithelial cells

Purification of colonic epithelial cells was performed as described[18].

Statistical Analysis

Data represent mean ± S.E.M. Where data were normally distributed, two-tailed Student's *t* test was used to determine significance in experiments with only two groups, and one-way ANOVA with the Newman-Keuls test was used to determine significant differences between multiple test groups. In Figure 4, the data were square root transformed to ensure normal distribution prior to statistical analysis. In other cases where data were not normally distributed, a one-way ANOVA with Kruskal-Wallis test, followed by a Mann-Whitney *U* test, was performed. Please see Supplementary Table 5 for all relevant *P* values as determined by Kruskal-Wallis test. Statistical analysis of all weight loss curves was performed by two-way ANOVA with Bonferroni post-test. All statistics were performed in Prism 5.0 (GraphPad Software, San Diego, CA, USA). A P value of < 0.05 was considered significant.

Supplementary Material

Refer to Web version on PubMed Central for supplementary material.

ACKNOWLEDGEMENTS

CD3, CD45R, and CD31 staining was performed by the Vanderbilt University Medical Center Translational Pathology Shared Resource supported by NIH grant P30CA068485 and the Vanderbilt Mouse Metabolic Phenotyping Center, supported by NIH grant U24DK059637. Slide imaging and quantification was performed in the Digital Histology Shared Resource (www.mc.vanderbilt.edu/dhsr). This work was funded by NIH grants R01DK053620, R01AT004821, R01CA190612, P01CA116087, and P01CA028842 (K.T.W.), Veterans Affairs Merit Review grant I01BX001453 (K.T.W.), the Thomas F. Frist Sr. Endowment (K.T.W.), and the Vanderbilt Center for Mucosal Inflammation and Cancer (K.T.W.). The human TMA was supported by NIH grant P50CA095103 and the DDRC Tissue Morphology Subcore (NIH grant P30DK058404). D.M.H. was supported by T32GM008554 and F31DK10715. L.A.C. was supported by Veterans Affairs Career Development Award 1IK2BX002126.

REFERENCES

1. Global Burden of Disease Cancer C. Fitzmaurice C, Dicker D, Pain A, Hamavid H, Moradi-Lakeh M, et al. The Global Burden of Cancer 2013. JAMA Onc. 2015; 1:505–527.
2. Brower V. Feeding the flame: new research adds to role of inflammation in cancer development. J Natl Cancer Inst. 2005; 97:251–253. [PubMed: 15713956]
3. Feagins LA, Souza RF, Spechler SJ. Carcinogenesis in IBD: potential targets for the prevention of colorectal cancer. Nat Rev Gastroenterol Hepatol. 2009; 6:297–305. [PubMed: 19404270]
4. Terzic J, Grivennikov S, Karin E, Karin M. Inflammation and colon cancer. Gastroenterology. 2010; 138:2101–2114. e2105. [PubMed: 20420949]
5. Martinez FO, Gordon S. The M1 and M2 paradigm of macrophage activation: Time for reassessment. F1000Prime Rep. 2014; 6:13. [PubMed: 24669294]
6. Mosser DM. The many faces of macrophage activation. J Leukoc Biol. 2003; 73:209–212. [PubMed: 12554797]

7. Mosser DM, Edwards JP. Exploring the full spectrum of macrophage activation. Nat Rev Immunol. 2008; 8:958–969. [PubMed: 19029990]
8. Erreni M, Mantovani A, Allavena P. Tumor-associated Macrophages (TAM) and Inflammation in Colorectal Cancer. Cancer Microenviron. 2011; 4:141–154. [PubMed: 21909876]
9. Isidro RA, Appleyard CB. Colonic macrophage polarization in homeostasis, inflammation, and cancer. Am J Physiol Gastrointest Liver Physiol. 2016; 311:G59–73. [PubMed: 27229123]
10. Anderson CF, Mosser DM. A novel phenotype for an activated macrophage: The type 2 activated macrophage. J Leukoc Biol. 2002; 72:101–106. [PubMed: 12101268]
11. Georgoudaki AM, Prokopec KE, Boura VF, Hellqvist E, Sohn S, Ostling J, et al. Reprogramming Tumor-Associated Macrophages by Antibody Targeting Inhibits Cancer Progression and Metastasis. Cell Rep. 2016; 15:2000–2011. [PubMed: 27210762]
12. Norton SE, Dunn ET, McCall JL, Munro F, Kemp RA. Gut macrophage phenotype is dependent on the tumor microenvironment in colorectal cancer. Clin Transl Immunol. 2016; 5:e76.
13. Greten FR, Eckmann L, Greten TF, Park JM, Li ZW, Egan LJ, et al. IKKbeta links inflammation and tumorigenesis in a mouse model of colitis-associated cancer. Cell. 2004; 118:285–296. [PubMed: 15294155]
14. Sakamoto K, Maeda S, Hikiba Y, Nakagawa H, Hayakawa Y, Shibata W, et al. Constitutive NF-kappaB activation in colorectal carcinoma plays a key role in angiogenesis, promoting tumor growth. Clin Cancer Res. 2009; 15:2248–2258. [PubMed: 19276252]
15. Xie W, Li M, Xu N, Lv Q, Huang N, He J, et al. MiR-181a regulates inflammation responses in monocytes and macrophages. PloS One. 2013; 8:e58639. [PubMed: 23516523]
16. De Simone V, Franze E, Ronchetti G, Colantoni A, Fantini MC, Di Fusco D, et al. Th17-type cytokines, IL-6 and TNF-alpha synergistically activate STAT3 and NF-kB to promote colorectal cancer cell growth. Oncogene. 2015; 34:3493–3503. [PubMed: 25174402]
17. Yu H, Pardoll D, Jove R. STATs in cancer inflammation and immunity: a leading role for STAT3. Nat Rev Cancer. 2009; 9:798–809. [PubMed: 19851315]
18. Hardbower DM, Singh K, Asim M, Verriere TG, Olivares-Villagomez D, Barry DP, et al. EGFR regulates macrophage activation and function in bacterial infection. J Clin Invest. 2016; 126:3296–3312. [PubMed: 27482886]
19. Krasinskas AM. EGFR Signaling in Colorectal Carcinoma. Pathol Res Int. 2011; 2011:932932.
20. Markman B, Javier Ramos F, Capdevila J, Tabernero J. EGFR and KRAS in colorectal cancer. Adv Clin Chem. 2010; 51:71–119. [PubMed: 20857619]
21. Spano JP, Lagorce C, Atlan D, Milano G, Domont J, Benamouzig R, et al. Impact of EGFR expression on colorectal cancer patient prognosis and survival. Ann Oncol. 2005; 16:102–108. [PubMed: 15598946]
22. Sasaki T, Hiroki K, Yamashita Y. The role of epidermal growth factor receptor in cancer metastasis and microenvironment. BioMed Res Int. 2013; 2013:546318. [PubMed: 23986907]
23. Yang JL, Qu XJ, Russell PJ, Goldstein D. Regulation of epidermal growth factor receptor in human colon cancer cell lines by interferon alpha. Gut. 2004; 53:123–129. [PubMed: 14684586]
24. Katz JP, Perreault N, Goldstein BG, Actman L, McNally SR, Silberg DG, et al. Loss of Klf4 in mice causes altered proliferation and differentiation and precancerous changes in the adult stomach. Gastroenterology. 2005; 128:935–945. [PubMed: 15825076]
25. Parang B, Kaz AM, Barrett CW, Short SP, Ning W, Keating CE, et al. BVES regulates c-Myc stability via PP2A and suppresses colitis-induced tumourigenesis. Gut. 2016 Epub ahead of print.
26. Engstrom A, Erlandsson A, Delbro D, Wijkander J. Conditioned media from macrophages of M1, but not M2 phenotype, inhibit the proliferation of the colon cancer cell lines HT-29 and CACO-2. Int J Oncol. 2014; 44:385–392. [PubMed: 24296981]
27. De Robertis M, Massi E, Poeta ML, Carotti S, Morini S, Cecchetelli L, et al. The AOM/DSS murine model for the study of colon carcinogenesis: From pathways to diagnosis and therapy studies. J Carcinog. 2011; 10:9. [PubMed: 21483655]
28. West NR, McCuaig S, Franchini F, Powrie F. Emerging cytokine networks in colorectal cancer. Nat Rev Immunol. 2015; 15:615–629. [PubMed: 26358393]

29. Hiemisch H, Schutz G, Kaestner KH. Transcriptional regulation in endoderm development: characterization of an enhancer controlling Hnf3g expression by transgenesis and targeted mutagenesis. EMBO J. 1997; 16:3995–4006. [PubMed: 9233809]
30. Holmfeldt P, Ganuza M, Marathe H, He B, Hall T, Kang G, et al. Functional screen identifies regulators of murine hematopoietic stem cell repopulation. J Exp Med. 2016; 213:433–449. [PubMed: 26880577]
31. Barrett CW, Fingleton B, Williams A, Ning W, Fischer MA, Washington MK, et al. MTGR1 is required for tumorigenesis in the murine AOM/DSS colitis-associated carcinoma model. Cancer Res. 2011; 71:1302–1312. [PubMed: 21303973]
32. Chandrasekar B, Deobagkar-Lele M, Victor ES, Nandi D. Regulation of chemokines, CCL3 and CCL4, by interferon gamma and nitric oxide synthase 2 in mouse macrophages and during Salmonella enterica serovar typhimurium infection. J Infect Dis. 2013; 207:1556–1568. [PubMed: 23431040]
33. Porta C, Rimoldi M, Raes G, Brys L, Ghezzi P, Di Liberto D, et al. Tolerance and M2 (alternative) macrophage polarization are related processes orchestrated by p50 nuclear factor kappaB. Proc Natl Acad Sci. 2009; 106:14978–14983. [PubMed: 19706447]
34. Valbuena G, Bradford W, Walker DH. Expression analysis of the T-cell-targeting chemokines CXCL9 and CXCL10 in mice and humans with endothelial infections caused by rickettsiae of the spotted fever group. Am J Pathol. 2003; 163:1357–1369. [PubMed: 14507644]
35. Yu H, Yue X, Zhao Y, Li X, Wu L, Zhang C, et al. LIF negatively regulates tumour-suppressor p53 through Stat3/ID1/MDM2 in colorectal cancers. Nature Commun. 2014; 5:5218. [PubMed: 25323535]
36. Yue X, Wu L, Hu W. The regulation of leukemia inhibitory factor. Cancer Cell Microenviron. 2015; 2
37. Huaux F, Lo Re S, Giordano G, Uwambayinema F, Devosse R, Yakoub Y, et al. IL-1alpha induces CD11b(low) alveolar macrophage proliferation and maturation during granuloma formation. J Pathol. 2015; 235:698–709. [PubMed: 25421226]
38. Sweet MJ, Hume DA. CSF-1 as a regulator of macrophage activation and immune responses. Arch Immunol Ther Exp (Warsz). 2003; 51:169–177. [PubMed: 12894871]
39. Van Overmeire E, Stijlemans B, Heymann F, Keirsse J, Morias Y, Elkrim Y, et al. M-CSF and GM-CSF Receptor Signaling Differentially Regulate Monocyte Maturation and Macrophage Polarization in the Tumor Microenvironment. Cancer Res. 2016; 76:35–42. [PubMed: 26573801]
40. Wang N, Liang H, Zen K. Molecular mechanisms that influence the macrophage m1-m2 polarization balance. Front Immunol. 2014; 5:614. [PubMed: 25506346]
41. Singh K, Chaturvedi R, Asim M, Barry DP, Lewis ND, Vitek MP, et al. The apolipoprotein E-mimetic peptide COG112 inhibits the inflammatory response to Citrobacter rodentium in colonic epithelial cells by preventing NF-kappaB activation. J Biol Chem. 2008; 283:16752–16761. [PubMed: 18417477]
42. Hanahan D, Weinberg RA. The hallmarks of cancer. Cell. 2000; 100:57–70. [PubMed: 10647931]
43. Mousa L, Salem ME, Mikhail S. Biomarkers of Angiogenesis in Colorectal Cancer. Biomark Cancer. 2015; 7:13–19.
44. Rmali KA, Puntis MC, Jiang WG. Tumour-associated angiogenesis in human colorectal cancer. Colorec Dis. 2007; 9:3–14.
45. Hol J, Wilhelmsen L, Haraldsen G. The murine IL-8 homologues KC, MIP-2, and LIX are found in endothelial cytoplasmic granules but not in Weibel-Palade bodies. J Leukoc Biol. 2010; 87:501–508. [PubMed: 20007247]
46. Heidemann J, Ogawa H, Dwinell MB, Rafiee P, Maaser C, Gockel HR, et al. Angiogenic effects of interleukin 8 (CXCL8) in human intestinal microvascular endothelial cells are mediated by CXCR2. J Biol Chem. 2003; 278:8508–8515. [PubMed: 12496258]
47. Li A, Dubey S, Varney ML, Dave BJ, Singh RK. IL-8 directly enhanced endothelial cell survival, proliferation, and matrix metalloproteinases production and regulated angiogenesis. J Immunol. 2003; 170:3369–3376. [PubMed: 12626597]

48. Ning Y, Manegold PC, Hong YK, Zhang W, Pohl A, Lurje G, et al. Interleukin-8 is associated with proliferation, migration, angiogenesis and chemosensitivity in vitro and in vivo in colon cancer cell line models. Int J Cancer. 2011; 128:2038–2049. [PubMed: 20648559]

49. Angelo LS, Kurzrock R. Vascular endothelial growth factor and its relationship to inflammatory mediators. Clin Cancer Res. 2007; 13:2825–2830. [PubMed: 17504979]

50. Wu WK, Llewellyn OP, Bates DO, Nicholson LB, Dick AD. IL-10 regulation of macrophage VEGF production is dependent on macrophage polarisation and hypoxia. Immunobiol. 2010; 215:796–803.

51. Pusztaszeri MP, Seelentag W, Bosman FT. Immunohistochemical expression of endothelial markers CD31, CD34, von Willebrand factor, and Fli-1 in normal human tissues. J Histochem Cytochem. 2006; 54:385–395. [PubMed: 16234507]

52. Chaturvedi R, Asim M, Piazuelo MB, Yan F, Barry DP, Sierra JC, et al. Activation of EGFR and ErbB2 by *Helicobacter pylori* results in survival of gastric epithelial cells with DNA damage. Gastroenterology. 2014; 146:1739–1751. [PubMed: 24530706]

53. Nicholson RI, Gee JMW, Harper ME. EGFR and cancer prognosis. Eur J Cancer. 2001; 37:9–15. [PubMed: 11165124]

54. Scaltriti M, Baselga J. The epidermal growth factor receptor pathway: A model for targeted therapy. Clin Cancer Res. 2006; 12:5268–5272. [PubMed: 17000658]

55. Dube PE, Yan F, Punit S, Girish N, McElroy SJ, Washington MK, et al. Epidermal growth factor receptor inhibits colitis-associated cancer in mice. J Clin Invest. 2012; 122:2780–2792. [PubMed: 22772467]

56. Kanneganti M, Mino-Kenudson M, Mizoguchi E. Animal models of colitis-associated carcinogenesis. J Biomed Biotechnol. 2011; 2011:342637. [PubMed: 21274454]

57. Uronis JM, Muhlbauer M, Herfarth HH, Rubinas TC, Jones GS, Jobin C. Modulation of the intestinal microbiota alters colitis-associated colorectal cancer susceptibility. PloS One. 2009; 4:e6026. [PubMed: 19551144]

58. Payne CM, Bernstein C, Bernstein H, Gerner EW, Garewal H. Reactive nitrogen species in colon carcinogenesis. Antioxid Redox Sig. 1999; 1:449–467.

59. Hardbower DM, Asim M, Murray-Stewart T, Casero RA Jr. Verriere T, Lewis ND, et al. Arginase 2 deletion leads to enhanced M1 macrophage activation and upregulated polyamine metabolism in response to *Helicobacter pylori* infection. Amino Acids. 2016; 48:2375–2388. [PubMed: 27074721]

60. Shibata W, Takaishi S, Muthupalani S, Pritchard DM, Whary MT, Rogers AB, et al. Conditional deletion of IkappaB-kinase-beta accelerates *Helicobacter*-dependent gastric apoptosis, proliferation, and preneoplasia. Gastroenterology. 2010; 138:1022–1034. e1021-1010. [PubMed: 19962981]

61. Parang B, Barrett CW, Williams CS. AOM/DSS Model of Colitis-Associated Cancer. Met Mol Biol. 2016; 1422:297–307.

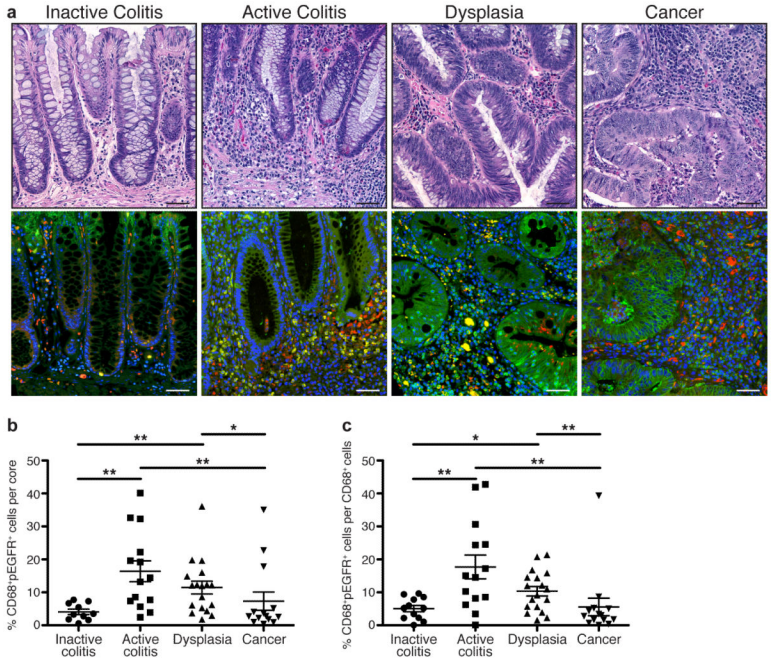

Figure 1. Macrophages have high levels of pEGFR Y1068 during inflammation driven, pre-cancerous stages of inflammatory bowel disease (IBD)-associated-colorectal cancer in human colonic tissues

(a) Representative hematoxylin and eosin (H&E)-stained images and representative immunofluorescence images of colonic tissues from the Vanderbilt University Medical Center IBD-associated colorectal cancer TMA. Red = CD68. Green = pEGFR Y1068. Yellow = Merge. Blue = DAPI. Scale bars = 50 μm. (b) Quantification of the percentage of $CD68^{+}pEGFR^{+}$ cells among the total number of cells in each individual core in the TMA, as determined by CellProfiler. (c) Quantification of the percentage of $CD68^{+}pEGFR^{+}$ cells among the total number of $CD68^{+}$ cells in each individual core in the TMA. For (a-c), $n = 10$ inactive colitis (normal or quiescent histology) samples, 14 active colitis (mild, moderate or severe histology) samples, 18 dysplasia samples, and 14 colorectal cancer samples. For (b-c), $*P < 0.05$, $**P < 0.01$ by one-way ANOVA with Kruskal-Wallis test, followed by Mann-Whitney *U* test.

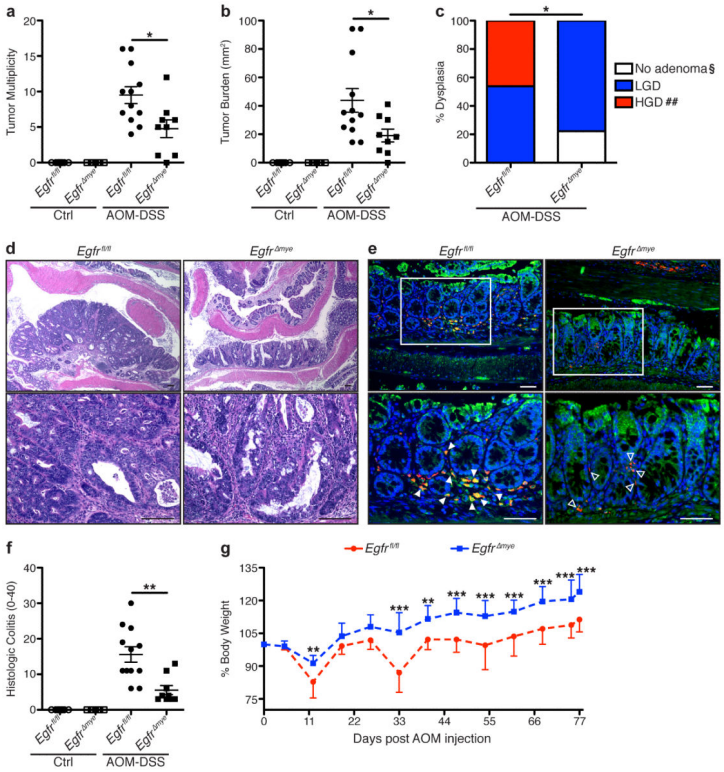

Figure 2. *Egfr*$^{\Delta mye}$ mice are significantly protected from tumorigenesis and dysplasia in the AOM-DSS model of colon tumorigenesis

(a) Tumor multiplicity was assessed by gross visual inspection, utilizing a dissecting microscope. (b) Tumor burden was determined by the addition of the calculated area of each identified tumor, as assessed with an electronic caliper for both length and width. (c) Percentage of cases with either no adenoma, low-grade dysplasia (LGD), and high-grade dysplasia (HGD) determined by a gastrointestinal pathologist (M.K.W.) in a blinded manner. By Chi Square test, *$P < 0.05$. §$P < 0.05$ versus *Egfr*$^{fl/fl}$; ##$P < 0.01$ versus *Egfr*$^{fl/fl}$. n = 9-12 AOM-DSS-treated animals per genotype. (d) Representative H&E-stained images from AOM-DSS-treated mice. Scale bars = 100 μm. (e) Representative immunofluorescence images of tEGFR from AOM-DSS-treated mice. Red = CD68. Green = tEGFR. Yellow = Merge. Blue = DAPI. Scale bars = 50 μm. Solid arrows indicate CD68^{+}tEGFR^{+} macrophages. Open arrows indicate CD68^{+}tEGFR^{-} macrophages. White box indicates zoomed area. n = ≥ 3 mice per genotype assessed. (f) Histologic colitis was determined by M.K.W. (g) Percentage of initial body weight was assessed at the indicated time points. *$P <$ 0.05, **$P < 0.01$, ***$P < 0.001$ versus *Egfr*$^{fl/fl}$ AOM-DSS by two-way ANOVA with Bonferroni post-test (ANOVA significance = $P < 0.001$). In (a), (b), and (f), *P < 0.05, **P < 0.01 by one-way ANOVA with Kruskal-Wallis test, followed by Mann-Whitney *U* test. In (a), (b), (f), and (g), n = 7-9 control and 9-12 AOM-DSS-treated mice per genotype.

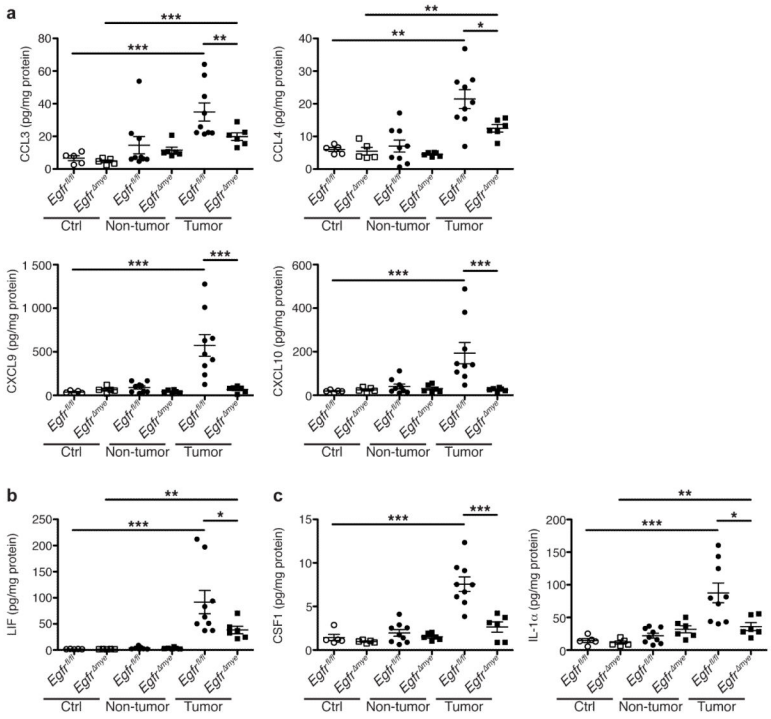

Figure 3. *Egfr*$^{\Delta mye}$ mice have significantly decreased cytokine and chemokine production within colon tumors

In a-c, protein levels were assessed by Luminex Multiplex Array from colonic tissues a 77 days post-AOM injection. (a) Levels of the C-C motif and C-X-C motif chemokines CCL3 (MIP-1α), CCL4 (MIP-1β), CXCL9 (MIG), and CXCL10 (IP-10). (b) Levels of the pleiotropic cytokine, LIF. (c) Levels of cytokines produced by activated macrophages, CSF1 (M-CSF) and IL-1α. In all panels, $*P < 0.05$, $**P < 0.01$, $***P < 0.001$ by one-way ANOVA with Kruskal-Wallis test, followed by Mann-Whitney *U* test. In all panels, $n = 5$ control tissues and 6-9 tumors with paired non-tumor area per genotype.

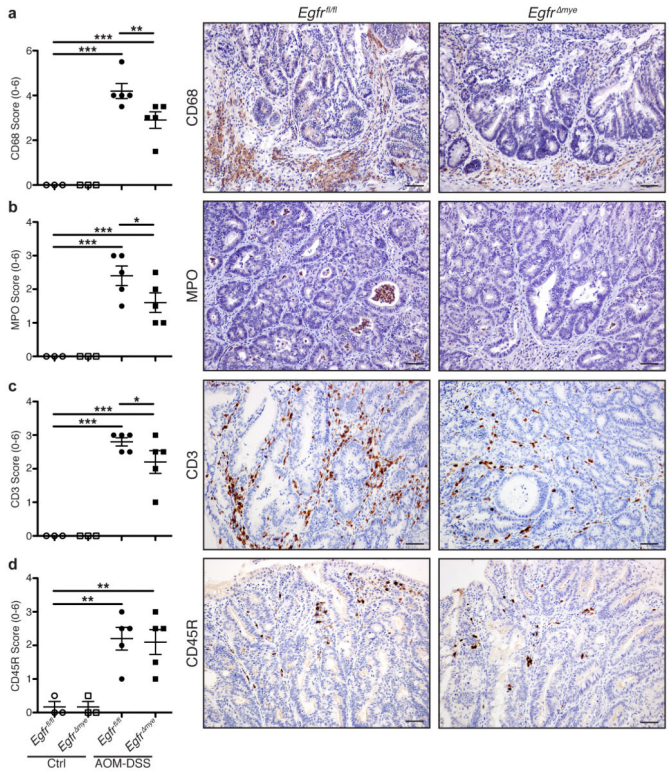

Figure 4. *Egfr*$^{\Delta mye}$ mice have significantly decreased macrophage, neutrophil and T cell infiltration during AOM-DSS treatment

(a) Quantification of CD68^{+} macrophage abundance with representative immunoperoxidase images of CD68 staining in AOM-DSS-treated mice. (b) Quantification of myeloperoxidase^{+} (MPO) neutrophil abundance with representative immunoperoxidase images of MPO staining in AOM-DSS-treated mice. (c) Quantification of CD3^{+} T cell abundance with representative immunoperoxidase images of CD3 staining in AOM-DSS-treated mice. (d) Quantification of CD45R^{+} B cell abundance with representative immunoperoxidase images of CD45R staining in AOM-DSS-treated mice. Scoring of immune cell abundance was performed by M.B.P. as described Materials and Methods. In all panels, scale bars = 50 μm. In all panels, $n = 3$ control and 5 AOM-DSS-treated mice per genotype. In all panels, *$P < 0.05$, **$P < 0.01$, ***$P < 0.001$ by one-way ANOVA with Newman-Keuls post-test after the data were square-root transformed.

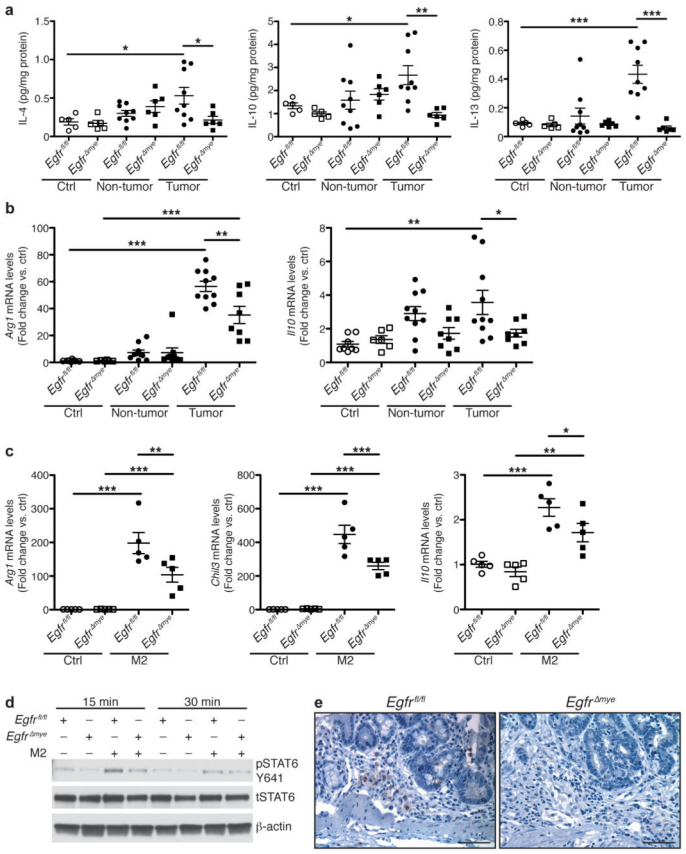

Figure 5. *Egfr*$^{\Delta mye}$ mice demonstrate decreased M2 macrophage activation during colon tumorigenesis

(a) Protein levels of the M2 stimuli, IL-4, IL-10, and IL-13, were assessed by Luminex Multiplex Array from colonic tissues 77 days post-AOM injection. $n = 5$ control tissues and 6-9 tumors with paired non-tumor area per genotype. (b) mRNA levels of M2 markers, *Arg1* and *Il10*, were assessed by qRT-PCR from colonic tissues 77 days post-AOM injection. $n =$ 6-8 control tissues and 8-10 tumors with paired non-tumor area per genotype. In (a) and (b), $*P < 0.05$, $**P < 0.01$, $***P < 0.001$ by one-way ANOVA with Kruskal-Wallis test, followed by Mann-Whitney U test. (c) mRNA levels of M2 markers, *Arg1*, *Chil3*, and *Il10*, were assessed by qRT-PCR in BMmacs 24 h post-treatment with classical M2 stimuli, IL-4 (10 ng/mL) and IL-10 (10 ng/mL). $n = 5$ biological replicates per genotype. In (c), $*P < 0.05$, $**P < 0.01$, $***P < 0.001$ by one-way ANOVA with Newman-Keuls post-test. (d) Representative western blot of pSTAT6 levels in BMmacs stimulated with the M2 stimulus, IL-4 (10 ng/mL), for the indicated times. $n = 3$ biological replicates. (e) Representative images of pSTAT6 immunoperoxidase staining in AOM-DSS-treated tissues. Scale bar = 50 μm. $n = 3$ mice per genotype.

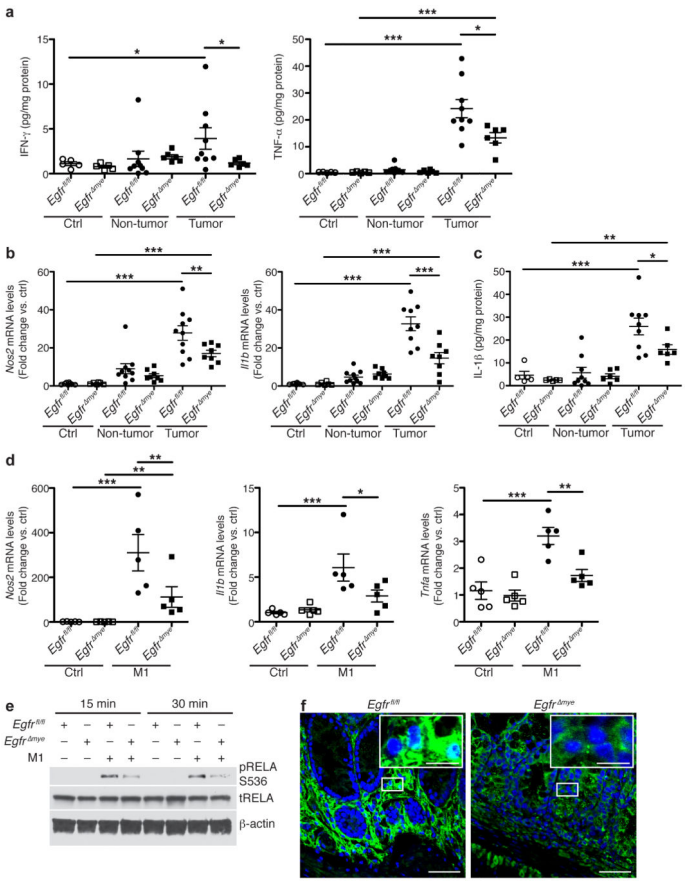

Figure 6. *Egfr*$^{\Delta mye}$ mice demonstrate decreased M1 macrophage activation during colon tumorigenesis

(a) Protein levels of M1 stimuli, IFN-γ and TNF-α, were assessed by Luminex Multiplex Array from colonic tissues 77 days post-AOM injection. $n = 5$ control tissues and 6-9 tumors with paired non-tumor area per genotype. (b) mRNA levels of M1 markers, *Nos2* and *Il1b*, were assessed by qRT-PCR from colonic tissues 77 days post-AOM injection. $n = 6$-8 control tissues and 8-10 tumors with paired non-tumor area per genotype. (c) Protein levels of the M1 marker, IL-1β, were assessed by Luminex Multiplex Array from colonic tissues 77 days post-AOM injection. $n = 5$ control tissues and 6-9 tumors with paired non-tumor area per genotype. In (a-c), $*P < 0.05$, $**P < 0.01$, $***P < 0.001$ by one-way ANOVA with Kruskal-Wallis test, followed by Mann-Whitney *U* test. (d) mRNA levels of M1 markers, *Nos2*, *Il1b*, and *Tnfa*, were assessed by qRT-PCR in bone marrow derived macrophages (BMmacs) 24 h post-treatment with classical M1 stimuli, IFN-γ (200 U/mL) and TNF-α (10 ng/mL). $n = 5$ biological replicates per genotype. In (d), $*P < 0.05$, $**P < 0.01$, $***P < 0.001$ by one-way ANOVA with Newman-Keuls post-test. (e) Representative western blot of pRELA (pp65) levels in BMmacs stimulated with the M1 stimuli, IFN-γ (200 U/mL) and lipopolysaccharide (10 ng/mL), for the indicated times. $n = 3$ biological replicates. (e) Representative confocal immunofluorescence images of cytoplasmic and nuclear RELA (p65) in AOM-DSS-treated tissues. Green = cytoplasmic RELA. White/Aqua = nuclear RELA. Blue = DAPI. Scale bar = 40 μm, Scale bar in inset = 10 μm. $n = 3$ mice per genotype.

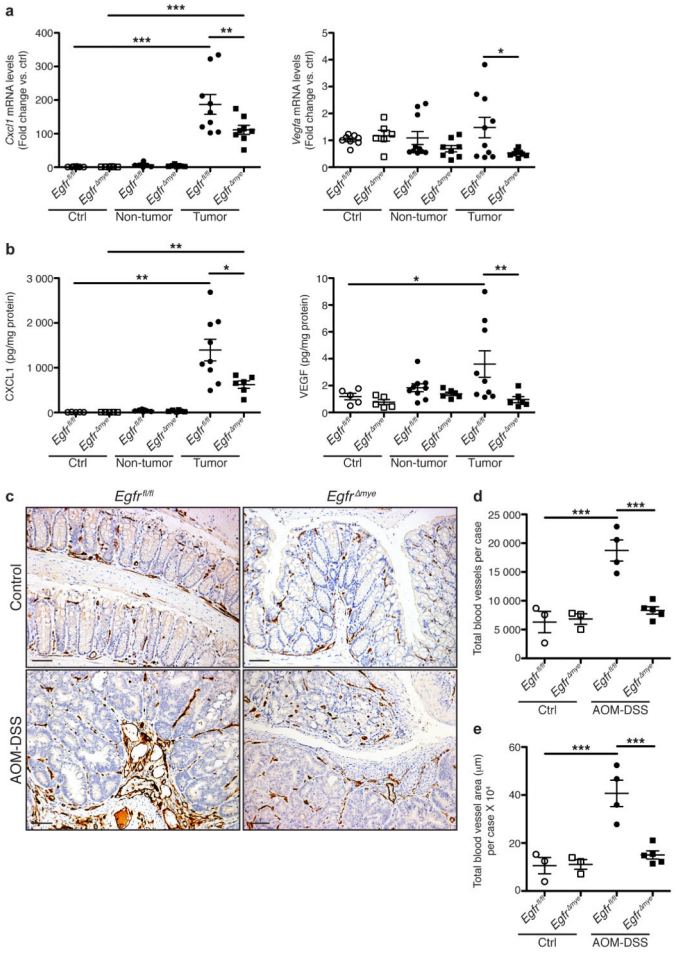

Figure 7. *Egfr*$^{\Delta mye}$ mice demonstrate decreased pro-angiogenic chemokine/cytokine production and angiogenesis during colon tumorigenesis

(a) mRNA levels of the pro-angiogenic chemokine, *Cxcl1*, and the pro-angiogenic cytokine, *Vegfa*, were assessed by qRT-PCR from colonic tissues 77 days post-AOM injection. n = 6-8 control tissues and 8-10 tumors with paired non-tumor area per genotype. (b) Protein levels of pro-angiogenic chemokine, CXCL1, and pro-angiogenic cytokine, VEGF, were assessed by Luminex Multiplex Array from colonic tissues 77 days post-AOM injection. n = 5 control tissues and 6-9 tumors with paired non-tumor area per genotype. In (a) and (b), *P < 0.05, **P < 0.01, ***P < 0.001 by one-way ANOVA with Kruskal-Wallis test, followed by Mann-Whitney U test. (c) Representative images of CD31$^+$ blood vessel immunohistochemistry in colonic tissues. Scale bars = 50 μm. (d) Quantification of the total number of CD31$^+$ blood vessels in (c). n = 3 control colonic tissues and 4-5 AOM-DSS-treated colonic tissues per genotype. (e) Quantification of the total CD31$^+$ blood vessel area within tissues in (c). n = 3 control colonic tissues and 4-5 AOM-DSS-treated colonic tissues per genotype. In (d) and (e), ***P < 0.001 by one-way ANOVA with Newman-Keuls post-test.